Sodium-Ion Batteries

Deutsche Ausgabe: DOI: 10.1002/ange.201411917
Internationale Ausgabe: DOI: 10.1002/anie.201411917

Ruthenium-Oxide-Coated Sodium Vanadium Fluorophosphate Nanowires as High-Power Cathode Materials for Sodium-Ion Batteries**

Manhua Peng, Biao Li, Huijun Yan, Dongtang Zhang, Xiayan Wang, Dingguo Xia,* and Guangsheng Guo*

Abstract: *Sodium-ion batteries are a very promising alternative to lithium-ion batteries because of their reliance on an abundant supply of sodium salts, environmental benignity, and low cost. However, the low rate capability and poor long-term stability still hinder their practical application. A cathode material, formed of RuO_2-coated $Na_3V_2O_2(PO_4)_2F$ nanowires, has a 50 nm diameter with the space group of I4/mmm. When used as a cathode material for Na-ion batteries, a reversible capacity of 120 mAh g^{-1} at 1 C and 95 mAh g^{-1} at 20 C can be achieved after 1000 charge–discharge cycles. The ultrahigh rate capability and enhanced cycling stability are comparable with high performance lithium cathodes. Combining first principles computational investigation with experimental observations, the excellent performance can be attributed to the uniform and highly conductive RuO_2 coating and the preferred growth of the (002) plane in the $Na_3V_2O_2(PO_4)_2F$ nanowires.*

With the development of renewable energy sources, sodium-ion batteries (SIBs) have attracted attention because of their low cost and the abundant sources of sodium when compared to lithium and lithium-ion batteries.[1] Considerable attention has been paid to explore the intercalation hosts for Na ions, such as Na_xCoO_2,[2] Na_xCrO_2,[3] Na_xFeO_2,[4] P2-$Na_x[Fe_{1/2}Mn_{1/2}]O_2$,[5] O3-$Na[Ni_{1/3}Fe_{1/3}Mn_{1/3}]O_2$,[6] and $Na_{2.24}FePO_4CO_3$.[7] Among them, fluorophosphates with a Na super ionic conductor (NASICON)-type structure have been proposed as promising cathode materials for SIBs because of their highly covalent three-dimensional crystalline structure, good thermal stability, and high energy density.[8] However, several critical problems are still suffered in the preparation and application of $Na_3V_2O_2(PO_4)2F$ including the larger particle size and the poor intrinsic electrical conductivity.[9–11]

In recent years, well-designed nanomaterials have been considered promising approaches to enhance the intercalation–deintercalation rates because of the short distances for Na-ion transport and their high surface-to-bulk ratio.[12] Many studies have been conducted on the synthesis of nanoscale low-dimensional cathode materials such as nanoparticles or nanoplates to improve the rate capability and cycling stability.[13] However, to date the reported $Na_3V_2O_2(PO_4)_2F$ compounds have a size range of micrometers or sub-micrometers,[9–11,14] which shows a more inferior rate performance in comparison with those of high-performance lithium cathodes. According to our knowledge, there have been no reports on $Na_3V_2O_2(PO_4)_2F$ wires tens of nanometers in diameter with the polymorph of *I4/mmm*. Moreover, the evidence of reaction mechanism evolution and detailed theoretical studies focused on $Na_3V_2O_2(PO_4)_2F$ with the space group of *I4/mmm* still could not be obtained.

Herein, we report the preparation of ruthenium oxide coated sodium vanadium fluorophosphate ($Na_3V_2O_2(PO_4)_2F$) nanowires by microemulsion-mediated hydrothermal synthesis. The morphology of $Na_3V_2O_2(PO_4)_2F$ can be easily controlled by adjusting the pH value of the solution. When used as a cathode for SIBs, the RuO_2-coated $Na_3V_2O_2(PO_4)_2F$ nanowires demonstrated an outstanding high-rate performance with a reversible specific capacity of 120 mAh g^{-1} at 1 C and 95 mAh g^{-1} at 20 C after 1000 cycles. The high-rate performance was comparable with that of high-performance lithium cathodes. The first principles computation discloses that preferred growth along the (002) plane is favorable to the diffusion of Na ions at high rate for $Na_3V_2O_2(PO_4)_2F$.

Depending on the pH value, which was controlled by adding drops of nitric acid to the precursor microemulsion, $Na_3V_2O_2(PO_4)_2F$ with different morphologies were synthesized. When a mixed solution with pH 2–3 was hydrothermally annealed at 180 °C for 24 h, the resulting $Na_3V_2O_2(PO_4)_2F$ nanowires were coated with amorphous RuO_2 to produce RuO_2-coated $Na_3V_2O_2(PO_4)_2F$ core–shell nanowires. Details of the procedure are described in the Experimental Section.

Figure 1 a shows the X-ray diffraction (XRD) pattern of the sample obtained at pH 2–3, which can be indexed to the tetragonal $Na_3V_2O_2(PO_4)_2F$ phase, demonstrating that a pure

[*] M. Peng, D. Zhang, Prof. X. Wang, Prof. G. Guo
Beijing Key Laboratory for Green Catalysis and Separation
Department of Chemistry and Chemical Engineering
Beijing University of Technology, Beijing 100124 (P.R. China)
E-mail: xiayanwang@bjut.edu.cn
B. Li, H. Yan, Prof. D. Xia
Beijing Key Laboratory for Theory and Technology of Advanced Battery Materials, College of Engineering
Peking University, Beijing 100871 (P.R. China)
E-mail: dgxia@pku.edu.cn

[**] This work was financially supported by the National Natural Science Foundation of China (No. 11179001), National High Technology Research and Development Program (No.2012AA052201), Excellent Young Scientists Fund of NSFC (No. 21322501), and Program for New Century Excellent Talents in University (NCET-12-0603). We would also like to acknowledge the staff of the XAS beamlines of the Beijing Synchrotron Radiation Facility.

Supporting information for this article is available on the WWW under http://dx.doi.org/10.1002/anie.201411917.

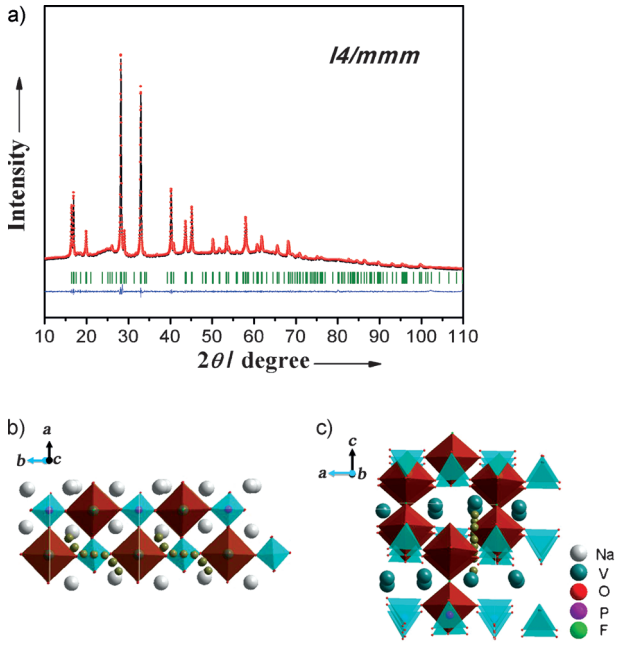

Figure 1. a) XRD patterns and Rietveld refinements of the $Na_3V_2O_2(PO_4)_2F$ powder; the experimental data are represented by the black line, the calculated pattern is represented by the red points, the Bragg positions are indicated by the green bars, and the difference curve is represented by the blue line. b), c) Rietveld refinement crystal structure of the $Na_3V_2O_2(PO_4)_2F$ powder in the b) *ab*-plane and c) *ac*-plane (the yellowish-green circles represent the diffusion paths).

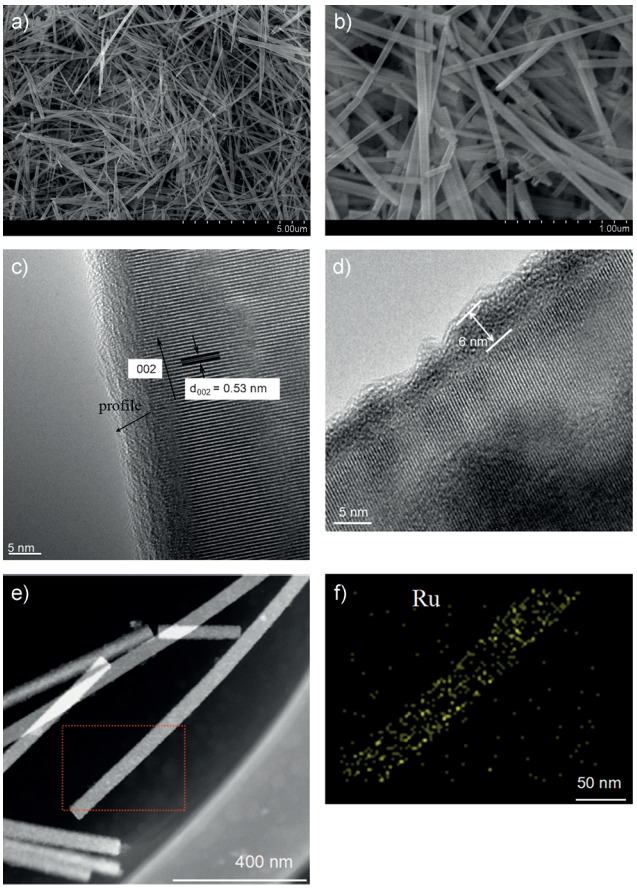

Figure 2. SEM images of $Na_3V_2O_2(PO_4)_2F$ nanowires with space group *I*4/*mmm* at a) low magnification (×10000) and b) high magnification (×50000). c) HRTEM image of the $Na_3V_2O_2(PO_4)_2F$ nanowires. d) HRTEM image of the RuO_2-coated $Na_3V_2O_2(PO_4)_2F$ nanowires with a 6 nm RuO_2 layer. e) A scanning transmission electron microscope (STEM) image of RuO_2-coated $Na_3V_2O_2(PO_4)_2F$ nanowires; f) The Ru mapping on the surface of RuO_2-coated $Na_3V_2O_2(PO_4)_2F$ nanowires.

and single-phased crystal was synthesized. The refined pattern shows that it had lattice parameters of $a = b = 6.4958$ Å and $c = 10.61366$ Å, with a space group of *I*4/*mmm*, which is different from the result reported by Sauvage et al.[11] The $Na_3V_2O_2(PO_4)_2F$ phases obtained at different pH values also showed the same XRD patterns (Supporting Information, Figure S1), indicating that they all consisted of tetrahedral $[PO_4]$ and octahedral $[VO_5F]$ units. The octahedral $[VO_5F]$ units shared a F atom with each other along the *c*-direction. The tetrahedral $[PO_4]$ and $[VO_5F]$ octahedral units were connected by an O atom in the *ab*-plane, which can be considered as a pseudolayered structure with intercalated Na ions on the *ab*-plane.[11] Based on the results of Rietveld analysis, Figure 1 b, c show the possible Na diffusion paths: the *ab*-plane and along the *c*-axis from a Na1 site to a neighboring Na1 site. The activation barriers were calculated by first principles to be 0.415 eV in the *ab*-plane and 2.248 eV in the *c*-axis direction (Supporting Information, Figure S2a, b). The values suggest that the Na-ion diffusion path was favorable along the *ab*-plane, that is, the (002) plane, indicating that $Na_3V_2O_2(PO_4)_2F$ with space group *I*4/*mmm* was a two-dimensional diffusion path.

The scanning electron microscope (SEM) image in Figure 2 a shows that $Na_3V_2O_2(PO_4)_2F$ nanowires were obtained at pH 2–3. Increasing the pH value of the mixed precursor solution resulted in a morphological change of the samples, such as the nanorods obtained at pH 3–5 and the nanosheets obtained at pH 5–7 (Supporting Information, Figure S3a, b). The $Na_3V_2O_2(PO_4)_2F$ nanowires had lengths of more than several micrometers. In the enlarged SEM image of the $Na_3V_2O_2(PO_4)_2F$ nanowires, shown in Figure 2 b, it can be seen that most of the nanowires had diameters in the range of about 50 nm. The high-resolution transmission electron microscope (HRTEM) image in Figure 2 c shows that the distances between the neighboring lattice fringes had an approximate value of 5.3 Å, which corresponds to the *d*-spacing of the (002) plane of the fluorophosphates. The change in morphology with the pH value at 180 °C can be explained as follows. Under the hydrothermal conditions at pH 2, a positively charged Na ion could be immediately adsorbed onto the negatively charged molecular clusters, which had been self-assembled along the normal direction of the basal (002) plane, by pillaring the Na ions.[15] The interfacial free energy of the (002) plane of the $Na_3V_2O_2(PO_4)_2F$ nanowires perpendicular to the *c*-axis was much higher than that of the other surfaces. $Na_3V_2O_2(PO_4)_2F$ could thus grow with an anisotropic crystal structure as one-dimensional nanowires in high-chemical-potential surroundings.[16] Since the Na ion diffusion paths were perpendicular to the nanowire growth direction, the preferred growth along

the (002) plane was favorable to the diffusion of Na ions at high rate.

Each $Na_3V_2O_2(PO_4)_2F$ nanowire was further coated with a RuO_2 shell to improve its sodium-storage performance using hydrolysis precipitation, followed by post-deposition annealing in ambient air. Figure 2d shows a TEM image of the RuO_2-coated $Na_3V_2O_2(PO_4)_2F$ nanowires. The core–shell structure with a shell thickness of 6 nm can be clearly distinguished. The results of scanning transmission electron microscope (STEM) and energy-dispersive X-ray spectroscopy (EDS) further confirmed the uniform existence of Ru on the surface (Figure 2e,f; Supporting Information, Figures S4a and S5). Furthermore, the $Na_3V_2O_2(PO_4)_2F$ nanowires coated with RuO_2 shells of different thickness are also shown in the Supporting Information, Figure S4b–d. Because each wire was one-dimensional, it was easy to establish line-to-line contact between the core and shell, which would enhance the electrical contact and ion or electron transfer relative to the point-to-point contact in powder electrodes.[17] Such a well-organized nanoscale core–shell structure could provide a high specific area, significantly reduce the inert zones, promote the diffusion of sodium ions, and thus enhance the rate properties.[18] Moreover, the ruthenium K-edge X-ray absorption near-edge structure (XANES) spectra (Supporting Information, Figure S6) show the white line for the RuO_2 coating shifting toward lower values relative to that of commercial RuO_2, which means that the valence state of ruthenium in the RuO_2 coating was lower than the standard valence of Ru^{IV}. According to the principle of electrical neutrality, the ruthenium oxide was oxygen-deficient in response to the formation of a surface coating with high electrical conductivity.[19] Therefore, an enhanced rate performance of RuO_2-coated $Na_2V_2O_2(PO_4)_2F$ nanowires was expected.

The specific capacity of $Na_3V_2O_2(PO_4)_2F$ with different morphologies was obtained (Supporting Information, Figures S7 and S8). The pristine $Na_3V_2O_2(PO_4)_2F$ nanowires delivered a maximum capacity of 101 mAh g^{-1} compared with the capacity of 83 mAh g^{-1} of nanorods and 75 mAh g^{-1} of nanosheets at 1 C, suggesting that the pristine $Na_3V_2O_2(PO_4)_2F$ nanowires exhibited enhanced rate performance. After the nanowires were coated with RuO_2, the capacity increased as expected. The cycling stability was almost the same for all of the nanowires with different coating thickness in the initial cycles, while the sample with a coating thickness of 6 nm delivered a maximum capacity of 120 mAh g^{-1} at 1 C and 95 mAh g^{-1} at 20 C. Hereafter, the data under discussion correspond to only those of RuO_2-coated $Na_3V_2O_2(PO_4)_2F$ nanowires with a coating thickness of 6 nm. Figure 3a exhibits the charge and discharge profiles of RuO_2-coated $Na_3V_2O_2(PO_4)_2F$ nanowires at a current density of 0.1 C in the voltage range of 2.5–4.3 V versus Na^+/Na. The initial discharge and charge specific capacities were 134 and 126 mAh g^{-1}, respectively, based on the total mass of the RuO_2-coated $Na_3V_2O_2(PO_4)_2F$ nanowires. The initial coulombic efficiency was as high as 94.0%. After 1000 cycles, the electrode could still deliver a reversible specific capacity of 95 mAh g^{-1} with a coulombic efficiency of 99.3% at a current rate of 20 C (Figure 3b). The cyclic voltammetry (CV) curves of RuO_2-coated $Na_3V_2O_2(PO_4)_2F$ nanowires and uncoated $Na_3V_2O_2(PO_4)_2F$ nanowires at different scan rate (Supporting Information, Figure S9) also demonstrate the excellent reversibility of the former. Figure 3c shows that the RuO_2-coated $Na_3V_2O_2(PO_4)_2F$ nanowires had a better rate performance compared with $Na_3V_2O_2(PO_4)_2F$ nanowires under all investigated current densities. Under a current density that was as high as 20 C, the nanowires without RuO_2 coating showed almost no capacity because of the intrinsic poor electrical conductivity, while the RuO_2-coated $Na_3V_2O_2(PO_4)_2F$ nanowires still exhibited a favorable initial specific capacity of 105 mAh g^{-1} at 20 C and 71 mAh g^{-1} at 40 C. The high-rate behavior can be attributed to the RuO_2 coating with uniformly high conductivity and the preferred growth of the (002) plane in the $Na_2V_2O_2(PO_4)_2F$ nanowires.

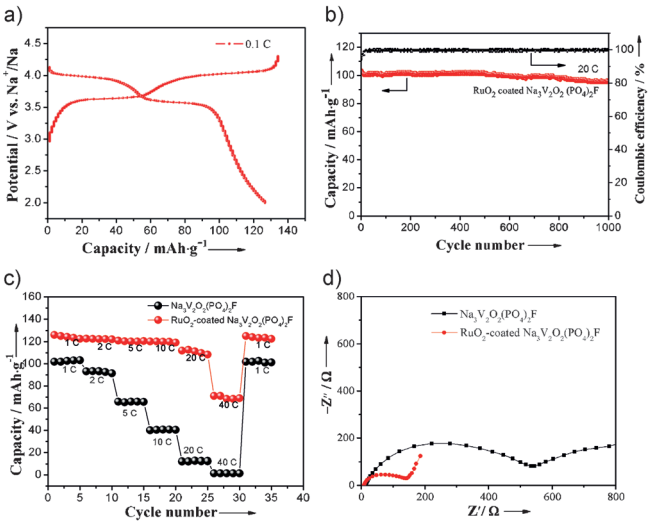

Figure 3. a) Charge and discharge profiles of RuO_2-coated $Na_3V_2O_2(PO_4)_2F$ nanowires at a current density of 0.1 C in the voltage range of 2.5–4.3 V versus Na^+/Na. b) Long-term cycling performance of the RuO_2-coated $Na_3V_2O_2(PO_4)_2F$ nanowires at a current density of 20 C. c) Rate capacity of RuO_2-coated $Na_3V_2O_2(PO_4)_2F$ nanowires and uncoated $Na_3V_2O_2(PO_4)_2F$ nanowires. d) Comparison between the Nyquist plots of the RuO_2 coated and uncoated $Na_3V_2O_2(PO_4)_2F$ nanowires.

Electrochemical impedance spectroscopy (EIS) was employed to further understand the origin of the enhanced electrochemical performance after the $Na_3V_2O_2(PO_4)_2F$ nanowires were coated by RuO_2. Figure 3d compares the Nyquist plots of the RuO_2-coated and uncoated $Na_3V_2O_2(PO_4)_2F$ nanowires. Based on the modified Randles equivalent circuit (Supporting Information, Figure S10a), the RuO_2-coated $Na_3V_2O_2(PO_4)_2F$ electrode showed a minimum charge-transfer resistance of 106.1 Ω compared to the value of 468.4 Ω for the electrode made of uncoated $Na_3V_2O_2(PO_4)_2F$ nanowires. This result indicates that the RuO_2-coated $Na_3V_2O_2(PO_4)_2F$ electrode had high electrical conductivity, resulting in the better rate capability and higher reversible capacity than those of the electrode of uncoated $Na_3V_2O_2(PO_4)_2F$ nanowires. The charge-transfer resistance became higher with increasing thickness of the RuO_2 coating (Supporting Information, Figure S10b) because the thicker coating suppressed charge transport.[20]

Ex situ XRD tests were performed to check the structural evolution of RuO_2-coated $Na_3V_2O_2(PO_4)_2F$ composites during charging and discharging; the results are shown in Figure 4. It can be seen that the XRD patterns of the

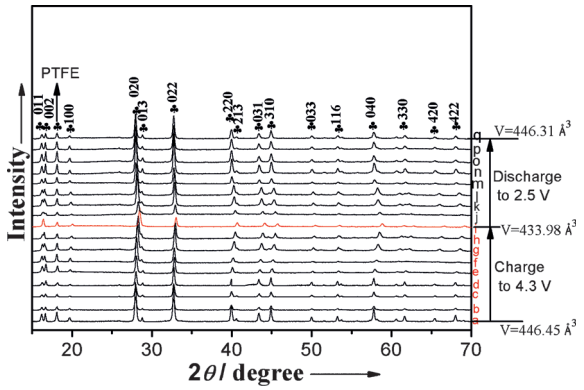

Figure 4. Ex situ XRD results of RuO_2-coated $Na_3V_2O_2(PO_4)_2F$ composites during charging (XRD patterns at voltages of 2.5,3.0, 3.60, 3.63, 3.76, 3.97, 4.02, 4.05, and 4.3 V) and discharging (XRD pattern at voltages of 4.05, 4.0, 3.98, 3.76, 3.60, 3.55, 3.52, and 2.5 V).

electrodes are similar to that of the as-prepared $Na_3V_2O_2(PO_4)_2F$ powder (Figure 1 a), apart from variations in intensity of some diffraction peaks during the charge–discharge process. Upon closer observation, during the charging process, the diffraction peaks at 16.28° and 16.76° consistently overlapped, the peaks at 28.86° vanished, and the peaks at 28.01°, 31.40°, 40.62°, 43.43°, and 44.95° shifted positively, and the diffraction peaks shifted back to original positions during the discharging process. This shift in peak positions was related to the change in lattice parameters. It is worth noting that no new phase appeared during charging and discharging, suggesting that the process involved a simple single-phase reaction of the $Na_3V_2O_2(PO_4)_2F$ electrode. A sustained decrease in lattice parameter *a* (the lattice parameter *a* is equal to *b*) is shown in the Supporting Information, Figure S11. Conversely, the lattice parameter *c* continues to increase over the whole process of charging. Besides, the rate of change in the lattice parameters (*a,b)* is lower than the lattice parameter *c* during charging (Supporting Information, Figure S11, inset), meaning that the distortion between the *ab* plane is larger than that within the *ab* plane upon Na ion intercalation or deintercalation.

Moreover, the volume change of 2.79% for $Na_3V_2O_2(PO_4)_2F$ at the end of the charging process is also smaller than that of olivine Na_xFePO_4 (ca. 17.5%),[21] $Na_xV_2(PO_4)_3$ (ca. 8.1%),[22] and $Na_xFe_3(PO_4)_2(P_2O_7$ (ca. 5.1%),[23] resulting in excellent cycling performance.

In conclusion, we have developed a new strategy to fabricate a promising structure of a circa 50 nm-diameter RuO_2-coated $Na_3V_2O_2(PO_4)_2F$ nanowires with the *I*4/*mmm* space group. As a cathode material for Na-ion batteries, the nanocomposite exhibited excellent cycling performance and rate capability in comparison with uncoated $Na_3V_2O_2(PO_4)_2F$ that can be attributed to the electronically conductive RuO_2, the growth of nanowires in a preferred orientation, and the small volume change during charging. This enhanced strategy and theoretical direction could offer an effective and basic approach to improving the cyclability and rate capability of sodium-ion electrode materials.

Experimental Section

$Na_3V_2O_2(PO_4)_2F$ nanowires were prepared by microemulsion-mediated hydrothermal synthesis.[24] A microemulsion consisting of cetyltrimethylammonium bromide (CTAB), water, cyclohexane, and *n*-pentanol was selected as the nanoreaction system. $C_2H_2O_4$ (analytical reagent (AR) grade), NaF (AR grade), $NH_4H_2PO_4$ (AR grade), and NH_4VO_3 (AR grade) were dissolved in the molar ratio 3:2:2:3 in deionized water to form a 0.2 mol L^{-1} dark-blue stabilized solution. A transparent mixed solution of CTAB (2 g, AR grade), cyclohexane (50 mL), and *n*-pentanol (2 mL) was prepared by vigorous stirring. These two solutions (mol ratio of water/surfactant = 5:1) were mixed together with substantial stirring to form a transparent microemulsion, and its pH value was adjusted to approximately 2–3 with HNO_3. The resulting transparent microemulsion was transferred into a 100 mL Teflon-lined stainless-steel autoclave and tightly sealed with heating at 180 °C for 24 h. The gray–black powder produced was collected through suction filtration. After washing several times with deionized water and ethanol, the powder particles were dried overnight in a vacuum oven set at 80 °C.

The RuO_2-coated $Na_3V_2O_2(PO_4)_2F$ core–shell nanowires were synthesized as follows. Anhydrous $RuCl_3$ (1 g, AR grade, Shanghai Ourchem Chemical Reagent Co., Ltd, China) was dissolved in about 96 mL of deionized water to form a stabilized black solution. To coat the amorphous RuO_2 onto the $Na_3V_2O_2$ $(PO_4)_2F$ nanowires, 0.75 mL of the black $RuCl_3$ solution was added to 20 mL of the $Na_3V_2O_2(PO_4)_2F$ suspension using a peristaltic pump at a uniform speed. The amount of RuO_2 in the synthesized RuO_2-coated $Na_3V_2O_2(PO_4)_2F$ core–shell nanowires was determined by inductively coupled plasma (ICP) to be similar to the theoretical quantity. The resultant gray-black powder was then collected by suction filtration. After washing several times with deionized water and ethanol, the powder particles were dried in air for 20 h in a tube furnace set at 150 °C.

More experimental and characterization details (for example, XRD, refined XRD, SEM, TEM, STEM-EDS mapping, and electrochemical characterization) are described in Supporting Information.

Keywords: fluorophosphates · nanowires · ruthenium oxide coating · sodium-ion batteries · vanadium

How to cite: *Angew. Chem. Int. Ed.* **2015**, *54*, 6452–6456
Angew. Chem. **2015**, *127*, 6552–6556

[1] S. Y. Hong, Y. Kim, Y. Park, A. Choi, N.-S. Choi, K. T. Lee, *Energy Environ. Sci.* **2013**, *6*, 2067–2081.
[2] R. Berthelot, D. Carlier, C. Delmas, *Nat. Mater.* **2011**, *10*, 74–80.
[3] S. Komaba, C. Takei, T. Nakayama, A. Ogata, N. Yabuuchi, *Electrochem. Commun.* **2010**, *12*, 355–358.
[4] J. Gaubicher, F. Boucher, P. Moreau, M. Cuisinier, P. Soudan, E. Elkaim, D. Guyomard, *Electrochem. Commun.* **2014**, *38*, 104–106.
[5] N. Yabuuchi, M. Kajiyama, J. Iwatate, H. Nishikawa, S. Hitomi, R. Okuyama, R. Usui, Y. Yamada, S. Komaba, *Nat. Mater.* **2012**, *11*, 512–517.
[6] M. Sathiya, K. Hemalatha, K. Ramesha, J.-M. Tarascon, A. S. Prakash, *Chem. Mater.* **2012**, *24*, 1846–1853.
[7] W. Huang, J. Zhou, B. Li, J. Ma, S. Tao, D. Xia, W. Chu, Z. Wu, *Sci. Rep.* **2014**, *4*, 4188.
[8] V. Palomares, M. C. Cabanas, E. Castillo-Martinez, M. H. Han, T. Rojo, *Energy Environ. Sci.* **2013**, *6*, 2312–2337.

[9] a) P. Serras, V. Palomares, P. Kubiak, L. Lezama, T. Rojo, *Electrochem. Commun.* **2013**, *34*, 344 – 347; b) P. Serras, V. Palomares, A. Goñi, P. Kubiak, T. Rojo, *J. Power Sources* **2013**, *241*, 56 – 60.
[10] M. Xu, L. Wang, X. Zhao, J. Song, H. Xie, Y. Lua, J. Goodenough, *Phys. Chem. Chem. Phys.* **2013**, *15*, 13032.
[11] F. Sauvage, E. Quarez, J.-M. Tarascon, E. Baudrin, *Solid State Sci.* **2006**, *8*, 1215 – 1221.
[12] K. Saravanan, C. W. Mason, A. Rudola, K. H. Wong, P. Balaya, *Adv. Energy Mater.* **2013**, *3*, 444 – 450.
[13] C. Zhu, K. Song, P. Aken, J. Maier, Y. Yu, *Nano Lett.* **2014**, *14*, 2175 – 2180.
[14] Y. Park, D. Seo, H. Kwon, B. Kim, J. Kim, H. Kim, I. Kim, H. Yoo, K. Kang, *J. Am. Chem. Soc.* **2013**, *135*, 13870 – 13878.
[15] Q. Wei, Q. An, D. Chen, L. Mai, S. Chen, Y. Zhao, K. M. Hercule, L. Xu, A. Minhas-Khan, Q. Zhang, *Nano Lett.* **2014**, *14*, 1042 – 1048.
[16] Y.-P. Fang, A.-W. Xu, R.-Q. Song, H.-X. Zhang, L.-P. You, J. C. Yu, H.-Q. Liu, *J. Am. Chem. Soc.* **2003**, *125*, 16025 – 16034.
[17] a) B. Wang, X. Li, X. Zhang, B. Luo, Y. Zhang, L. Zhi, *Adv. Mater.* **2013**, *25*, 3560 – 3565; b) H. Wu, G. Zheng, N. Liu, T. J. Carney, Y. Yang, Y. Cui, *Nano Lett.* **2012**, *12*, 904 – 909.
[18] C. Zhu, Y. Yu, L. Gu, K. Weichert, J. Maier, *Angew. Chem. Int. Ed.* **2011**, *50*, 6278 – 6282; *Angew. Chem.* **2011**, *123*, 6402 – 6406.
[19] Q. Fu, W.-X. Li, Y. Yao, H. Liu, H.-Y. Su, D. Ma, X.-K. Gu, L. Chen, Z. Wang, H. Zhang, B. Wang, X. Bao, *Science* **2010**, *328*, 1141 – 1144.
[20] L. Zhao, Y.-S. Hu, H. Li, Z. Wang, L. Chen, *Adv. Mater.* **2011**, *23*, 1385 – 1388.
[21] P. Moreau, D. Guyomard, J. Gaubicher, F. Boucher, *Chem. Mater.* **2010**, *22*, 4126 – 4128.
[22] Z. Jian, W. Han, X. Lu, H. Yang, Y.-S. Hu, J. Zhou, Z. Zhou, J. Li, W. Chen, D. Chen, L. Chen, *Adv. Energy Mater.* **2013**, *3*, 156 – 160.
[23] H. Kim, I. Park, D.-H. Seo, S. Lee, S.-W. Kim, W. J. Kwon, Y.-U. Park, C. S. Kim, S. Jeon, K. Kang, *J. Am. Chem. Soc.* **2012**, *134*, 10369 – 10372.
[24] M. Cao, C. Hu, E. Wang, *J. Am. Chem. Soc.* **2003**, *125*, 11196 – 11197.

Received: December 12, 2014
Published online: April 9, 2015

